THE JOURNAL OF BIOLOGICAL CHEMISTRY VOL. 283, NO. 46, pp. 32045–32055, November 14, 2008

Structure of the Human SENP7 Catalytic Domain and Poly-SUMO Deconjugation Activities for SENP6 and SENP7*[S]

Received for publication, July 23, 2008, and in revised form, September 3, 2008 Published, JBC Papers in Press, September 16, 2008, DOI 10.1074/jbc.M805655200

Christopher D. Lima[‡1] **and David Reverter**[§2]

From the [‡]*Structural Biology Program, Sloan-Kettering Institute, New York, New York 10065 and* [§]*Institut de Biotecnologia i de Biomedicina, Universitat Autonoma de Barcelona, 08193 Bellaterra, Barcelona, Spain*

Small ubiquitin-like modifier (SUMO) proteases regulate the abundance and lifetime of SUMO-conjugated substrates by antagonizing reactions catalyzed by SUMO-conjugating enzymes. Six SUMO proteases constitute the human SENP/ULP protease family (SENP1–3 and SENP5–7). SENP6 and SENP7 include the most divergent class of SUMO proteases, which also includes the yeast enzyme ULP2. We present the crystal structure of the SENP7 catalytic domain at a resolution of 2.4 Å. Comparison with structures of human SENP1 and SENP2 reveals unique elements that differ from previously characterized structures of SUMO-deconjugating enzymes. Biochemical assays show that SENP6 and SENP7 prefer SUMO2 or SUMO3 in deconjugation reactions with rates comparable with those catalyzed by SENP2, particularly during cleavage of di-SUMO2, di-SUMO3, and poly-SUMO chains composed of SUMO2 or SUMO3. In contrast, SENP6 and SENP7 exhibit lower rates for processing pre-SUMO1, pre-SUMO2, or pre-SUMO3 in comparison with SENP2. Structure-guided mutational analysis reveals elements unique to the SENP6 and SENP7 subclass of SENP/ULP proteases that contribute to protease function during deconjugation of poly-SUMO chains.

Ubiquitin (Ub)[3] and ubiquitin-like (Ubl) proteins are conjugated to target proteins via an isopeptide bond between the Ub/Ubl C-terminal residue and a lysine residue on the protein target (1). Small ubiquitin-like modifier (SUMO) is one of the best characterized Ubls from among approximately one dozen Ubl family members identified to date (2, 3). The SUMO pathway contributes to the regulation of many cellular processes that include replication, nuclear transport, transcription, recombination, chromosome segregation, and cytokinesis (4).

The human SUMO protein family consists of three isoforms, SUMO1, SUMO2, and SUMO3 (see under "Experimental Procedures" for definition of SUMO nomenclature). Mature SUMO1 shares only 43% identity to SUMO2 or SUMO3, whereas SUMO2 and SUMO3 share greater than 95% identity at the primary amino acid level (and are thus referred to as SUMO2/3 in some instances). SUMO4 was recently identified as a fourth SUMO family member (5), although it remains unclear whether SUMO4 participates in formation of SUMO conjugates *in vivo* (6). A cascade of SUMO-specific E1-E2-E3 enzymes is required to promote SUMO conjugation, whereas SUMO-specific proteases are required to catalyze SUMO deconjugation (1–4, 7).

SUMO isoforms contribute to nonredundant functions in the cell as evidenced by the observation that some proteins appear modified exclusively with SUMO1 or SUMO2/3, whereas other substrates can be modified with either SUMO1 or SUMO2/3 (8, 9). In addition, SUMO1 and SUMO2/3 exhibit different dynamics *in vivo* in response to stimuli such as oxidative stress or heat shock (10–12). The most striking difference between SUMO1 and SUMO2/3 is that SUMO2/3 can form poly-SUMO2/3 chains via isopeptide bonds between SUMO2/3 N-terminal lysine residues and the C-terminal glycine from the next SUMO2/3 molecule. This feature is also shared with the yeast SUMO ortholog SMT3. In yeast, polymeric SMT3 chains are essential for synaptonemal complex assembly during meiotic chromosomal segregation (13), but they are not required for any essential function in yeast grown under vegetative conditions (14). Other evidence suggests that SUMO2/3 chains might contribute to Aβ production (15) and promyelocytic leukemia protein stability (16). More recently, poly-SUMO chains were proposed to recruit a ubiquitin ligase that targets the substrate or chains for ubiquitin-mediated proteolysis (*i.e.* SUMO-modified PML (17, 18)).

SUMO proteases contribute to two distinct activities in the cell, processing SUMO precursors to generate mature SUMO and deconjugation of SUMO-conjugated substrates to release mature SUMO and the respective substrate. Cleavage occurs after the conserved SUMO Gly-Gly motif either at the scissile peptide bond during processing or at the scissile isopeptide bond during deconjugation (7). SUMO proteases are called SENP in human and ULP in yeast. SENP/ULP proteins include conserved catalytic domains that are both necessary and sufficient to promote SUMO deconjugation and maturation activity *in vitro*. The human SENP protease family includes six family members termed SENP1, SENP2, SENP3, SENP5, SENP6, and SENP7 (19), each of which share between 20 and 60% sequence

* This work was supported, in whole or in part, by National Institutes of Health Grant GM65872 (to C. D. L.). This work was also supported by European Community Grant MIRG-CT-2007-200346 (to D. R.). The costs of publication of this article were defrayed in part by the payment of page charges. This article must therefore be hereby marked "*advertisement*" in accordance with 18 U.S.C. Section 1734 solely to indicate this fact.

[S] The on-line version of this article (available at http://www.jbc.org) contains supplemental Figs. 1–3.

[1] To whom correspondence may be addressed: Sloan-Kettering Institute, 1275 York Ave., New York, NY 10065. Tel.: 212-639-8205; Fax: 212-717-3047; E-mail: limac@mskcc.org.

[2] To whom correspondence may be addressed: Universitat Autonoma de Barcelona, 08193 Bellaterra, Barcelona, Spain. Tel.: (93) 581-1379, Fax: (93) 581-2011; E-mail: david.reverter@uab.cat.

[3] The abbreviations used are: Ub, ubiquitin; Ubl, Ub-like; r.m.s.d., root mean square deviation; SUMO, small ubiquitin-like modifier; PDB, Protein Data Bank.

identity to each other within their respective catalytic domains. SENP/ULP catalytic domains are not always specific for SUMO. Whereas human DEN1 shares some similarities with other SUMO protease catalytic domains (20–23), DEN1 exhibits low sequence similarity when compared with other SENP/ULP family members (13–15% identity) and is a NEDD8-specific protease.

Several recent reports suggest that SENP/ULP family members participate in nonredundant cellular functions. For instance, mouse SENP1 is required during embryonic development and is involved in the stabilization of the HIF1α during hypoxia (24, 25), whereas knockdown of SENP5 transcripts revealed essential functions during mitosis and/or cytokinesis as evidenced by defects in nuclear morphology and inhibition of cell proliferation (26). In addition to their catalytic domains, SUMO proteases include large N-terminal domains that share no similarity to one another. These domains can be as small as 355 amino acid residues for SENP3 and up to 663 for SENP7. In most instances it is thought that the SENP/ULP N-terminal domains direct subcellular localization (26–32) and that subcellular localization contributes in part to SENP/ULP function by restricting protease activity to distinct areas within the cell.

SENP/ULP family members also display unique proteolytic activities *in vitro* and *in vivo*. In mammalian cells, SENP6 preferentially processes SUMO2 and SUMO3 chains, and when SENP6 is depleted, SUMO2 and SUMO3 accumulate in PML nuclear bodies (32). SENP1 and SENP2 are the best characterized SENP/ULP proteases, and both are more adept at catalyzing deconjugation in comparison with processing (33–36). For example, SENP2 exhibits 15- or 112-fold higher specificity for deconjugation of SUMO2/3-RanGAP1 in comparison with processing pre-SUMO2 or pre-SUMO3, respectively (34). SENP1 lacks a clear preference for any particular SUMO isoform, whereas SENP2 exhibits a slight preference for SUMO2/3 over SUMO1.

SENP6 and SENP7 constitute the most divergent subclass within the SENP/ULP family, one that includes yeast ULP2 (19). In addition to lower sequence similarity within the catalytic domain, SENP6 and SENP7 include conserved sequence insertions in distinct positions within their catalytic domains. To characterize this subclass of SENP/ULP proteases, we conducted biochemical assays to evaluate the activities of SENP6 and SENP7 in comparison with SENP2. SENP6 and SENP7 exhibit specificity for SUMO2/3, especially when poly-SUMO2 or poly-SUMO3 chains are used as substrates. The x-ray structure for the SENP7 catalytic domain was determined at 2.4 Å, and structure-guided mutational analysis revealed unique elements conserved within SENP6 and SENP7 that contribute to substrate specificity and catalytic activity.

EXPERIMENTAL PROCEDURES

Protein Purification—The catalytic domains of human SENP6-(637–1112) and SENP7-(662–984) were amplified by PCR using human lung and brain PCR-ready cDNA (Ambion) and cloned into pET28b to encode a polypeptide fused to a thrombin-cleavable N-terminal hexa-histidine tag. Expression constructs were used to transform *Escherichia coli* BL21(DE3) codon plus cells (Novagen). Bacterial cultures were grown by fermentation at 37 °C to $A_{600} = 0.8$, and isopropyl-β-D-thiogalactopyranoside (IPTG) was added to a final concentration of 0.5 mM. Cultures were incubated for 3–4 h at 30 °C and harvested by centrifugation (7000 × *g*), and the supernatant was discarded. Cell suspensions were equilibrated in 20% sucrose, 20 mM Tris-HCl (pH 8.0), 1 mM β-mercaptoethanol, 350 mM NaCl, 20 mM imidazole, 10 μg/ml DNase, 1 mM phenylmethylsulfonyl fluoride, 0.1% IGEPAL CA-630, and 20 μg/ml lysozyme, and cells were disrupted by sonication. Cell debris was removed by centrifugation (40,000 × *g*). Protein was separated from lysate by metal affinity chromatography using nickel-nitrilotriacetic acid-agarose resin (Qiagen) and eluted with 25 mM Tris-HCl (pH 8.0), 350 mM NaCl, 300 mM imidazole, and 2 mM β-mercaptoethanol and dialyzed against buffer containing 25 mM Tris-HCl (pH 8.0), 200 mM NaCl, and 2 mM β-mercaptoethanol with thrombin (Sigma) at a 1:1000 ratio. After thrombin cleavage, fractions containing SENP6 and SENP7 were separated by gel filtration (Superdex 200; GE Healthcare). Fractions containing the protein of interest were pooled, diluted to 50 mM NaCl, applied to anion exchange resin (Mono Q; GE Healthcare), and eluted with a NaCl gradient from 0 to 50% of a buffer containing 25 mM Tris-HCl (pH 8.0), 1 M NaCl, and 2 mM β-mercaptoethanol in 12 column volumes. Fractions containing the protein of interest were pooled, concentrated to 10 mg/ml, and snap-frozen in liquid nitrogen prior to storage at −80 °C.

Single point mutations were introduced into the SENP7 coding region using the Quick-Change mutagenesis kit (Stratagene). PCR was used to construct SENP7 deletion mutants by fusing amino acids 684–693 (Loop-1 SENP7-Δ685–692), by substituting two glycine residues for the loop between residues 747 and 768 (Loop-2 SENP7-Δ748–767), and by fusing amino acids 810 to 862 (Loop-3 Δ811–861). All plasmids were confirmed by DNA sequencing. SENP7 wild-type and mutant isoforms were purified by metal affinity chromatography and gel filtration (as described above) and concentrated to 1 mg/ml in a buffer containing 25 mM Tris-HCl (pH 8.0), 350 mM NaCl, and 1 mM β-mercaptoethanol. SENP2, SUMO precursors, and RanGAP1-SUMO conjugates were produced as described previously (33, 34). Di-SUMO2, di-SUMO3, poly-SUMO2, and poly-SUMO3 chains were purchased from Boston Biochem. Swiss-Prot nomenclature was utilized for SUMO isoforms whereby pre-SUMO1 terminates with -GG-HSTV (UniProtKB Swiss-Prot, P63165), pre-SUMO2 terminates with -GG-VY (UniProtKB Swiss-Prot, P61956), and pre-SUMO3 terminates with -GG-VPESSLAGHSF (UniProtKB Swiss-Prot, P55854).

Biochemical and Kinetic Assays—All assays were conducted in triplicate. Error bars indicate ± 1 S.D. C-terminal hydrolase activity was measured by incubating pre-SUMO1, pre-SUMO2, and pre-SUMO3 proteins (5 μM) with purified SENP6 or SENP7 wild-type and SENP7 mutant isoforms at three different enzyme concentrations (0.5, 5, and 50 nM) at 23 °C in a buffer containing 25 mM Tris-HCl (pH 8.0), 150 mM NaCl, 0.1% Tween 20, and 2 mM dithiothreitol. Reactions were stopped after 10 min with SDS loading buffer and analyzed by gel electrophoresis (PAGE). Proteins were detected by staining with SYPRO or FLAMINGO (Bio-Rad). Identical experimental conditions were used to assay deconjugation activities for SENP2, SENP6, and SENP7 wild-type and mutant isoforms at 0.05, 0.5,

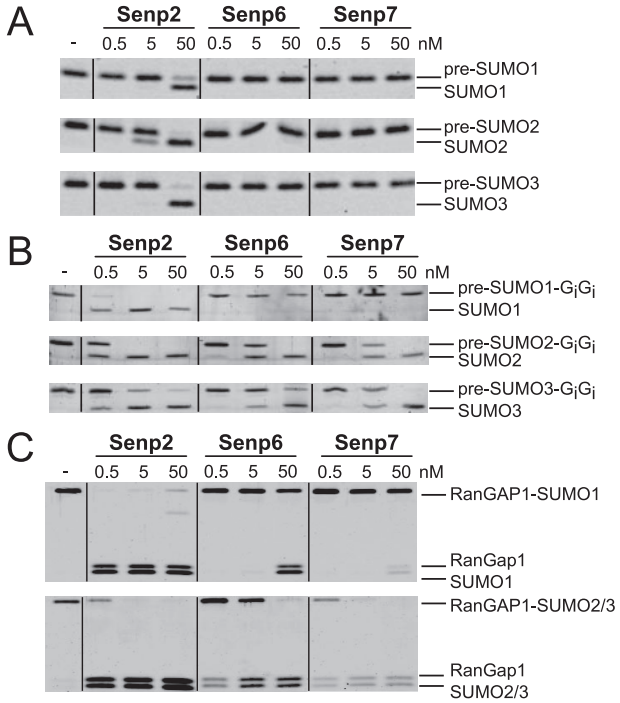

FIGURE 1. **Processing and deconjugation activities for SENP2, SENP6, and SENP7.** *A,* end point assays for SUMO processing catalyzed by SENP2, SENP6, and SENP7 at 0.5, 5, and 50 nM using pre-SUMO1, pre-SUMO2, and pre-SUMO3 at 5 μM. *B,* end point assays for SENP2, SENP6, and SENP7 at 0.5, 5, and 50 nM using pre-SUMO1, pre-SUMO2, and pre-SUMO3 at 5 μM in which two additional glycine residues (G_iG_i) were inserted C-terminal to the cleavage site. *C,* end point assays for SENP2, SENP6, and SENP7 at 0.5, 5, and 50 nM using the substrates RanGAP1-SUMO1 and RanGAP1-SUMO2/3. Reactions were stopped after 10 min with SDS loading buffer and analyzed by PAGE. Proteins were detected by staining with SYPRO or FLAMINGO (Bio-Rad).

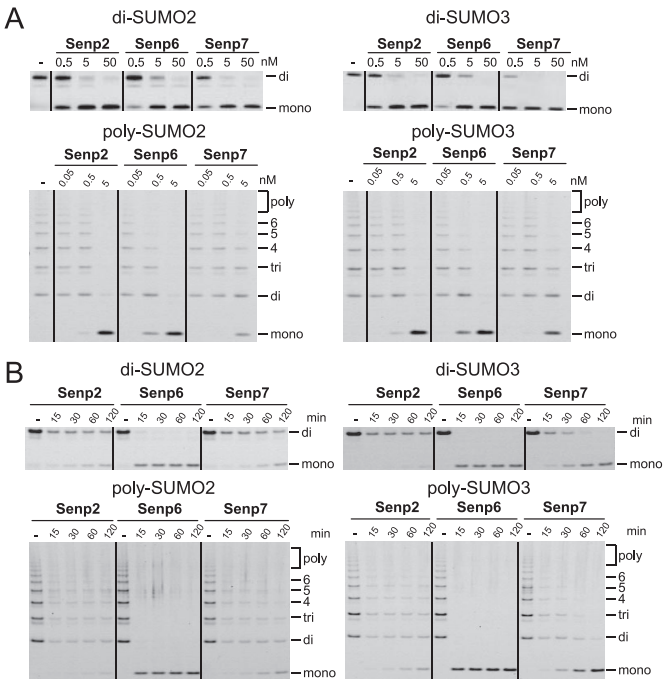

FIGURE 2. **Deconjugation activities for SENP2, SENP6, and SENP7 using poly-SUMO chains.** *A,* end point assays for SENP2, SENP6, and SENP7 at 0.5, 5, and 50 nM using di-SUMO2 and di-SUMO3 substrates at 2 μM (*upper panel*). End point deconjugation assays for SENP2, SENP6, and SENP7 at 0.05, 0.5, and 5 nM using poly-SUMO2 and poly-SUMO3 as substrates at 45 μg/ml (*lower panel*). *B,* time course assays to measure deconjugation catalyzed by SENP2, SENP6, and SENP7 at 0.5 nM using the substrates di-SUMO2 and di-SUMO3 at 2 μM (*upper panel*) or poly-SUMO2 and poly-SUMO3 at 45 μg/ml (*lower panel*). For end point assays, reactions were stopped after 10 min with SDS loading buffer and analyzed by PAGE. Proteins were detected by staining with SYPRO or FLAMINGO (Bio-Rad). For kinetic analysis, reactions were stopped at the respective time intervals indicated in minutes at the *top* of each panel.

5, and 50 nM using di-SUMO2, di-SUMO3, NΔ419RanGAP1-SUMO1, and NΔ419RanGAP1-SUMO2/3 at 2 μM. Because of the polydisperse nature of poly-SUMO substrates, we utilized poly-SUMO2 or poly-SUMO3 at 45 μg/ml, a concentration similar to that used for di-SUMO substrates (2 μM). Reactions were stopped after 10 min with SDS loading buffer and analyzed by PAGE. Proteins were detected by staining with SYPRO or FLAMINGO (Bio-Rad). Products were quantified by detecting fluorescence under UV illumination using a Gel-Doc apparatus with associated integration software (Quantity-One; Bio-Rad). Initial reaction velocities for deconjugation were measured for SENP7 wild-type and mutant isoforms using the di-SUMO2 substrate in a buffer containing 25 mM Tris-HCl (pH 8.0), 150 mM NaCl, 0.1% Tween 20, and 2 mM dithiothreitol. Reactions were stopped at indicated time intervals with SDS loading buffer and analyzed by PAGE. Proteins were detected by staining with SYPRO or FLAMINGO (Bio-Rad).

Crystallization and Data Collection—Crystals of the SENP7 catalytic domain were obtained at 18 °C by sitting drop vapor diffusion methods. The reservoir solution contained 1.6 M ammonium sulfate and 100 mM sodium citrate (pH 6.5). Single crystals appeared after 2 days from equal volumes of protein solution (10 mg/ml in 5 mM Tris-HCl (pH 8.0), 25 mM NaCl) and reservoir solution. Crystals were cryo-protected in reservoir buffer containing 12% glycerol and flash-frozen in liquid nitrogen prior to diffraction analysis. Diffraction data were recorded from cryo-cooled crystals (100 K) at APS beamline 24-IDC. Data were integrated, scaled, and merged using HKL2000 (37), reduced, and further analyzed using CCP4 (38) (Table 1).

Structure Determination and Refinement—The structure for the SENP7 catalytic domain was determined by multiple isomorphous replacement using x-ray diffraction data collected from two crystals incubated in either 0.5 mM mercury acetate or 0.5 mM thimerosal overnight in buffer containing 1.6 M ammonium sulfate, 100 mM sodium citrate (pH 6.5) prior to cryoprotection as described for the native crystal. Phases were calculated using diffraction data from the native and derivative data sets using the program SOLVE/RESOLVE (39). Experimental electron density was interpreted to build a model for the SENP7 catalytic domain using the program O (40) and Coot (41). Refinement utilized CNS (42) and REFMAC (38). Ramachandran analysis showed 96.7% of residues (233:241) in favored regions, 0.0% in outlier regions, and 100% of residues in allowed (241:241) regions (43). Refinement and data statistics are provided in Table 1.

Accession Codes Protein Data Bank—Coordinates and structure factors are deposited in the RCSB data bank with accession code 3EAY.

RESULTS

SENP6 and SENP7 Are SUMO2/3-specific and -deficient in SUMO Maturation—The SENP6 catalytic domain included amino acid residues 637–1112, whereas the SENP7 catalytic

domain included amino acids 662–984. For clarity, we will refer to these catalytic domain fragments as SENP6 and SENP7 throughout the remainder of the text. These protein preparations were assessed in biochemical assays to determine their ability to catalyze SUMO processing and SUMO deconjugation in comparison with SENP2 (see "Experimental Procedures"). Analysis of processing reactions containing SENP2, SENP6, and SENP7 at three different enzyme concentrations (0.5, 5, and 50 nM) suggested that SENP6 and SENP7 could not efficiently process SUMO1, SUMO2, or SUMO3 precursors under

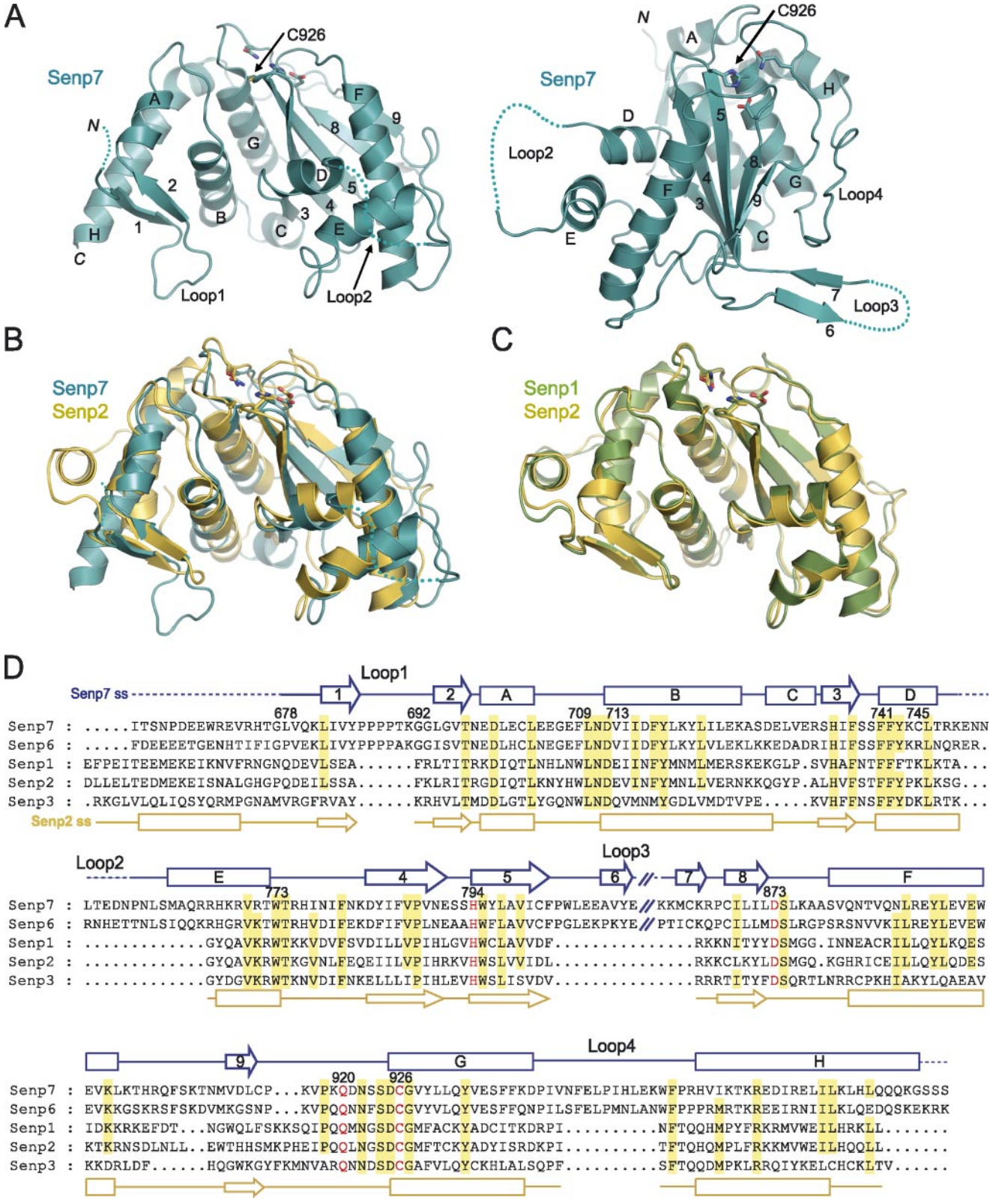

the conditions tested, although a very small amount of product was observed for SENP6 using the pre-SUMO2 substrate (Fig. 1*A*). The lack of activity observed for SENP6 and SENP7 is in stark contrast to the processing activities catalyzed by SENP2 (Fig. 1*A*) (33, 34) or SENP1 (35).

Previous characterization of the SENP2 and ULP1 proteases suggested that SUMO processing was dependent on the composition of amino acid side chains C-terminal to the conserved Gly-Gly motif and cleavage site (Fig. 1*B*) (33, 34). Interestingly, SUMO isoform specificity lessened and activities were enhanced for SENP2 and ULP1 using SUMO substrates that contained two additional glycine residues inserted C-terminal to the cleavage site (Gly-Gly-Gly_i-Gly_i-*X* where *X* is the remaining native sequence (see "Experimental Procedures") and Gly_i is the inserted glycine residue (33)). Similar to results obtained for SENP2 and ULP1, SENP6 and SENP7 exhibited higher processing activities when these SUMO precursors were used, but only for pre-SUMO2-GGG_iG_i-*X* and pre-SUMO3-GGG_iG_i-*X* (Fig. 1*B*).

These results suggest that SENP6 and SENP7 are poor enzymes for pre-SUMO processing but demonstrate that SENP6 and SENP7 exhibit specificity for SUMO2/3. To probe this specificity further, SENP6 and SENP7 were utilized in deconjugation reactions using SUMO1-RanGAP1 or SUMO3-RanGAP1 conjugates (Fig. 1*C*). These data suggest that SENP6 and SENP7 catalyze deconjugation of SUMO3-RanGAP1 at rates comparable with SENP2 under the conditions tested. In contrast to SENP2, SENP6 and SENP7 were less able to deconjugate SUMO1-RanGAP1, and products were only detected at enzyme concentrations 100× higher than that observed for reactions containing SENP2.

SENP6 and SENP7 Are Proficient at Deconjugating Di-SUMO2/3 and Poly-SUMO2/3 Chains—SENP6 was previously shown to dismantle poly-SUMO2 and poly-SUMO3 chains in a process that appeared critical for PML body maintenance (32). We next assessed SENP6 and SENP7 catalytic domains for their ability to promote deconjugation of di-SUMO2/3 or poly-SUMO2/3 chains using four distinct SUMO substrates as follows: di-SUMO2 and di-SUMO3, which contain two SUMO molecules linked covalently by an isopeptide bond between the C-terminal glycine in one SUMO and Lys-11 in the other molecule of SUMO; and poly-SUMO2 and poly-SUMO3, which are composed of chains containing between two and greater than eight SUMO molecules linked via the aforementioned isopeptide bond. Deconjugation assays utilized different enzyme concentrations for SENP2, SENP6, and SENP7 (0.05, 0.5, 5, and 50 nM) and fixed concentrations for respective substrates (see "Experimental Procedures"; Fig. 2*A*). In each case, cleavage products were observed for SENP2, SENP6, and SENP7, although SENP6 appeared to catalyze poly-SUMO2/3 deconjugation at faster rates in comparison with either SENP2 or SENP7. These differences can be best appreciated in Fig. 2*B,* which shows the kinetics of the reaction using 0.5 nM of the respective protease. In this instance, SENP6 and SENP7 were more adept at promoting cleavage of poly-SUMO2 or poly-SUMO3 in comparison with reactions containing SENP2. The intermediates observed in each reaction suggest that SENP2, SENP6, or SENP7 catalytic domains employ a distributive rather than processive mechanism to degrade SUMO chains.

Crystal Structure of Human SENP7—Crystals were obtained for the SENP7 catalytic domain that encompassed amino acid residues 662–984. Molecular replacement failed using available structures of SENP1 and SENP2, so the SENP7 structure was solved by multiple isomorphous replacement using crystals soaked in the presence of two mercury compounds, thimerosal or mercury acetate. The structure contains one molecule in the crystallographic asymmetric unit, and subsequent refinement produced a model that was refined to 2.4 Å with an *R*-factor and R_{free} of 20.2 and 25.6%, respectively (Fig. 3*A*, supplemental Fig. 1, *A* and *B*, and Table 1; see "Experimental Procedures").

The SENP7 structure revealed its relationship to the SENP/ULP protease family as well as to other members of the Cys-48 cysteine protease family (Fig. 3). However, the structure of the SENP7 catalytic domain also revealed features unique to this subfamily of SENP/ULP family members (Fig. 3). These differences include the following: (i) the absence of an N-terminal α-helix that is present in structures of SENP1, SENP2, and ULP1; (ii) four insertions that we have termed Loop-1, -2, -3, and -4; and (iii) several secondary structure elements unique or extended in SENP7 in comparison with SENP1 or SENP2. Consistent with these differences, SENP7 does not align well to SENP1 (r.m.s.d. of 2.0 Å over 182 aligned residues; 29% sequence identity) or SENP2 (r.m.s.d. of 2.0 Å over 187 aligned residues; 29% sequence identity) (Fig. 3*B*). In contrast, SENP1 and SENP2 exhibit much higher similarity and can be aligned with an r.m.s.d. of 0.8 Å over 224 residues with a sequence identity of 60% (Fig. 3*C*).

To determine whether structural differences observed for SENP7 could explain its specificity for SUMO2/3, di-SUMO2/3, or poly-SUMO2/3, we generated models for SENP7 in complex with SUMO using available structures of

FIGURE 3. **Structure of the catalytic domain of SENP7.** *A*, two views of the SENP7 catalytic domain shown in *ribbon* representation. Secondary structure elements are either numbered (β-strands) or lettered (α-helices). The catalytic residues are depicted in *stick* representation near the *top* of each panel, and the catalytic cysteine is labeled (*C926*). The insertion elements (Loop-1, Loop-2, Loop-3, and Loop-4) are labeled in at least one of the two panels. Segments of the polypeptide not observed in the electron density maps were deemed disordered and are indicated by *dashed lines*. The N and C termini are labeled *N* or *C*, respectively. *B,* superposition of the SENP7 and SENP2 (PDB 1THO) structures in ribbon representation with SENP7 colored *blue* and SENP2 colored *yellow*. Catalytic residues are shown in *stick* representation as in *A*. *C,* superposition of SENP1 (PDB 2IYC) with SENP2 (PDB 1THO) in *ribbon* representation with SENP1 colored *green* and SENP2 colored *yellow*. Catalytic residues are shown in *stick* representation. *D,* alignment of sequences corresponding to the catalytic domains for human SENP7, SENP6, SENP1, SENP2, and SENP3 based on structural alignment of human SENP2 and SENP7. Gaps are denoted by *dots* and the large sequence insertion within Loop-3 is depicted by // to indicate that the sequence is missing from the alignment. Numbering *above* the sequence alignment corresponds to the amino acid position in full-length SENP7. Secondary structural elements are indicated *above* the alignment for SENP7 (*blue*) and *below* the alignment for SENP2 (*yellow*). For SENP7, β-strands are numbered, α-helices lettered, and coil depicted as a *line*. Missing regions in our structure are denoted by *dashed lines*, and the *gap* in Loop-3 is indicated by //. Side chain identity (75% conservation) is denoted in the alignment by a *yellow background*. Conserved catalytic residues are depicted in *red*. Graphics were prepared with PYMOL (47).

TABLE 1

Crystallographic data

Data in parentheses indicate statistics for data in the highest resolution bin (2.49-2.4 Å).

	Native	Hg (thimerosal)	Hg (mercury acetate)
Source	APS 24-IDC	APS 24-IDC	APS 24-IDC
Wavelength	0.9795 Å	0.9795 Å	0.9795 Å
Resolution limits	40-2.4 Å (2.49-2.4 Å)	40-2.4 Å (2.49-2.4 Å)	40-2.4 Å (2.49-2.4 Å)
Space group	$P3_221$	$P3_221$	$P3_221$
Unit cell (*a, b, c,* α, β, γ)	76.2, 76.2, 103.5, 90, 90, 120	74.2, 74.2, 101.2, 90, 90, 120	73.5, 73.5, 101.1, 90, 90, 120
No. of observations	119,195	123,379	110,587
No. of reflections	14,050 (1380)	23,892 (2274)[a]	23380 (2258)[a]
Completeness	99.7% (99.9%)	98.6% (94.6%)[a]	99.0% (95.8%)[a]
Mean $I/\sigma I$	15.9 (4.0)	11.9 (1.7)[a]	15.4 (2.4)[a]
R_{merge} on I[b]	0.065 (0.302)	0.097 (0.453)[a]	0.081 (0.330)[a]
R_{pim} on I[c]	0.033 (0.188)	0.035 (0.192)[a]	0.036 (0.145)[a]
Cut-off criteria $I/\sigma I$	0	0	0
No. of Hg sites	0	3	2
FOM (SOLVE/RESOLVE)		0.35/0.56	
Refinement Statistics			
PDB ID	3EAY		
Resolution limits (Å)	40-2.4 (2.49-2.4)		
No. of reflections	13,901 (999)		
Protein atoms	2059		
Water/sulfate atoms	66/5		
R_{cryst}[d]/R_{free} (5% of data)	0.202 (0.309)/0.256 (0.359)		
Bond length r.m.s.d.	0.006 Å		
Bond angles r.m.s.d.	1.2°		
Average *B* factor (protein/water)	31.5/39.9		
Ramachandran statistics	233/241 (96.7%) in most favored 0/241 (0.0%) in disallowed 241/241 (100%) in allowed		

[a] Hg derivative data treats Bijvoët mates independently.
[b] $R_{merge} = \Sigma_{hkl}\,\Sigma_i|I(hkl)i - \langle I(hkl)\rangle|/\Sigma_{hkl}\Sigma_i\,\langle I(hkl)I\rangle$ (37).
[c] $R_{pim} = \Sigma_{hkl}(1/(N-1))^{1/2}\Sigma_i|I(hkl)i - \langle I(hkl)\rangle|/\Sigma_{hkl}\Sigma_i\,\langle I(hkl)I\rangle$ (48).
[d] $R_{cryst} = \Sigma_{hkl}|F_o(hkl) - F_c(hkl)|/\Sigma_{hkl}\,|F_o(hkl)|$, where F_o and F_c are observed and calculated structure factors, respectively.

SENP1 and SENP2 that were previously solved in complex with SUMO or SUMO-conjugated RanGAP1 (Fig. 4 and supplemental Fig. 1). Previous structural studies with SENP1, SENP2, and ULP1 revealed a bi-partite protease interface (site A) that dictates specificity for SUMO via an extensive protease interface that contacts SUMO at sites distal from the cleavage site (Fig. 4*B*) (33, 35, 44). Interactions from this region continue into the protease active site cleft where contacts are made to the SUMO C-terminal tail, Gly-Gly motif, and residues immediately C-terminal to the scissile peptide bond (Fig. 4*B*) (34, 35). Structures for complexes between SUMO-conjugated RanGAP1 and either SENP2 or SENP1 revealed the relative position for the substrate (site B) (34, 35). Based on the position of RanGAP1 in these structures, we modeled the relative position for a second molecule of SUMO if SENP7 were engaged in cleaving di-SUMO (Fig. 4*B*, *bottom panel*; supplemental Fig. 1).

Superposition of SENP7 with SENP2 revealed several interesting differences near the putative site A interface with SUMO (Fig. 4*A*) that included amino acid side chain substitutions in SENP7 (Phe-709, Val-713, and Cys-745) that differ from those conserved in both SENP2 (Trp-410, Glu-414, and Lys-445) and SENP1 (Figs. 3*D* and 4, *C* and *D*). Other interesting differences include the positions of Loop-1 and Loop-2 in SENP7, elements with no correlate in either SENP1 or SENP2. Loop-1 is located between β-strands 1 and 2 and is positioned to project toward SUMO in binding site A (Fig. 4, *A* and *D*). Loop-1 amino acid residues are highly conserved in both SENP6 and SENP7 (Fig. 3*D*). Loop-2 is located between helices D and E on the other side of site A relative to Loop-1 (Figs. 3*A* and 4*B*). Loop-2 includes a more loosely conserved insertion of ~15 amino acids in SENP6 and SENP7. In the SENP7 structure, eight Loop-2 residues (750–757) were not observed in the electron density.

Previous analysis of structures of ULP1-SMT3 and SENP2-SUMO1 suggested that several polar and charged residues contribute to complementary electrostatics in the interface between the protease and SUMO (33, 44). Electrostatic surfaces calculated for either SENP1 or SENP2 (Fig. 4*E*) appear similar and include an acidic patch (*red*) and basic patch (*blue*) on opposite sides of the interface with SUMO (*green circle*). Consistent with the differences noted above adjacent to site A, the electrostatic potential surface calculated for SENP7 appears quite distinct from that observed for SENP1 and SENP2. The acidic patch is largely neutralized and replaced in part by a basic patch on the SENP7 surface. Val-713 and Loop-1 contribute to the neutralization of this surface and to the basic patch that appears unique to SENP7 (Fig. 4*E*). Val-713 is conserved in SENP7 and SENP6 but substituted to glutamate in SENP1 and SENP2. Loop-1, which includes four consecutive proline residues (Pro-686, Pro-687, Pro-688, and Pro-689) followed by Thr-690, Lys-691, and three glycine residues (Gly-692, Gly-693, and Gly-695), has no correlate in SENP1 or SENP2 or other SENP/ULP family members (Figs. 3*D* and 4*D*).

In contrast to Loop-1 and Loop-2, which buttress the SUMO-binding surface near site A, Loop-3 and Loop-4 are located on the opposite surface of the protease catalytic domain (Figs. 3*A* and 4*B*). Loop-3 includes a large insertion of 63 amino acid residues between β5 and β8. In our structure, this insertion includes β6 and β7, although 50 amino acids of this element are disordered in our structure (812–861). In SENP6, this insertion is even larger and includes 194 amino acid residues. Based on

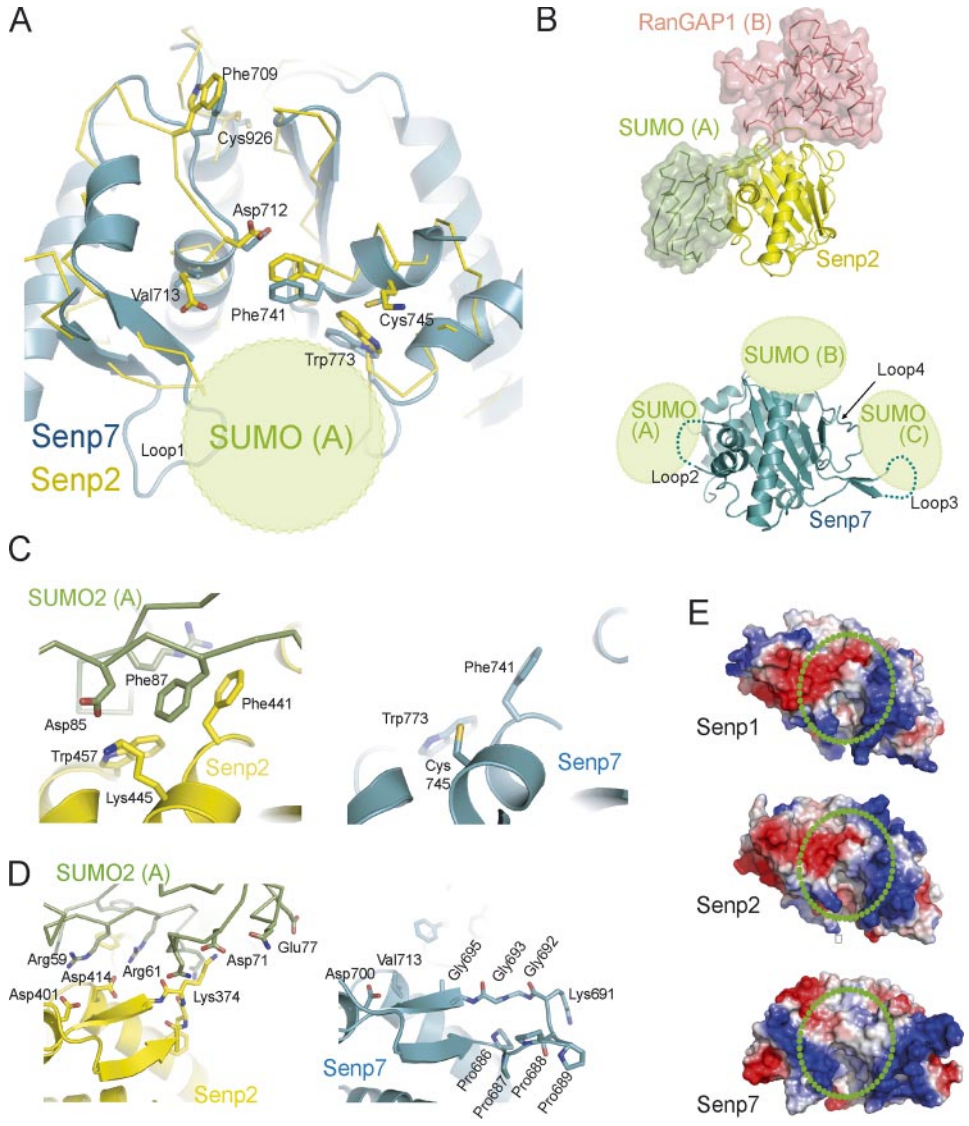

FIGURE 4. **Structural models for interactions between SENP7 and SUMO.** *A*, superposition of the SENP7 and SENP2 catalytic domains in *blue ribbon* and *yellow stick* representation, respectively. The position of SUMO is indicated schematically based on the position of SUMO2 in complex with SENP2 (PDB 2IO0). Several residues within the SUMO-protease interface are highlighted in *stick* representation and labeled according to their position and side chain composition in SENP7. *B*, *top panel*, the structure of SUMO2-RanGAP1 (*stick* and *transparent surface* representation) is shown in complex with SENP2 (*yellow ribbon* representation) to indicate the position of SUMO in site A (*green*) and the substrate RanGAP1 in site B (*pink*). The *bottom panel* depicts the SENP7 catalytic domain in a similar orientation to SENP2 in the *top panel* to highlight the positions of Loop-2, Loop-3, and Loop-4 with respect to the putative SUMO interaction surfaces in site A, site B, and site C. *C*, close-up view of the interface between SENP2 (*yellow*) and SUMO2 (*green*) with SENP7 (*blue*) shown at the *right* in an analogous orientation to highlight residues involved in interactions with SUMO at site A. *D*, similar to *C*, but depicting the other side of the SENP2-SUMO2 complex to highlight residues in SENP7 Loop-1 that may contribute to SUMO interaction. *E*, electrostatic potential surface representation for SENP1, SENP2, and SENP7 to highlight similarities between SENP1 and SENP2 within the SUMO interaction surface (site A) and the differences between SENP7 and either SENP1 or SENP2 in the analogous surface. The relative position for SUMO in site A is indicated by a *green circle* as derived from structures of SENP1-SUMO, SENP2-SUMO and models for SENP7-SUMO.

amino acid similarity, we predict that β6 and β7 would be present in SENP6, although the remaining elements of the insertion are not well conserved. Loop-4 is well conserved in SENP6 and SENP7 and fully observed in our SENP7 structure. Whereas Loop-3 and Loop-4 are too far from the substrate-binding surfaces to contribute to interactions in site A or site B as observed in structures obtained for SENP1 or SENP2 in complex with SUMO-RanGAP1 (Fig. 4*B, top*), Loop-3 and Loop-4 might contribute to interactions with a substrate in site C if SENP6 or SENP7 were to engage a poly-SUMO chain (Fig. 4*B, bottom*).

Mutagenesis and Biochemical Characterization of SENP7—Deletion and single-point substitutions were generated for the SENP7 catalytic domain to test whether the aforementioned structural features confer specificity for SUMO processing or deconjugation. Mutant isoforms included those that lacked Loop-1 (Δ685–692), Loop-2 (Δ748–767), or Loop-3 (Δ811–861) (see "Experimental Procedures"). We chose not to delete Loop-4 because it was well ordered and included side chains that contributed to the hydrophobic core in SENP7 (supplemental Fig. 1, *A* and *B*). In addition to loop deletions, single-point substitutions were generated for Phe-709, Val-713, and Cys-745. Phe-709 was selected for substitution because it is conserved as tryptophan in most SENP/ULP family members, a residue previously proposed as a specificity determinant for interaction with the SUMO C-terminal tail and Gly-Gly motif (Fig. 4*A*) (34). Val-713 and Cys-745 are located in the putative interface with SUMO, and these positions are conserved as glutamate and lysine, respectively, in SENP1 and SENP2 (Fig. 4, *C* and *D*). Each mutant SENP7 isoform behaved similarly to wild-type SENP7 during purification insofar as mutant isoforms eluted from gel filtration as mono-disperse peaks at positions consistent with their expected apparent molecular weight, although SENP7-V713E/C745K could not be readily separated from higher or lower molecular weight contaminants (see supplemental Fig. 2). Because each protein behaved as predicted, and because each preparation exhibited some catalytic activity, respective mutations did not appear to present substantive barriers to protein folding.

SENP7 isoforms containing deletions in Loop-1, Loop-2, and Loop-3 were compared with wild-type SENP7 in reactions for processing each of the three SUMO precursors (Fig. 5*A*). Titration experiments utilized three different protease concentrations (0.5, 5, and 50 nM) in the presence of 5 μM pre-SUMO1,

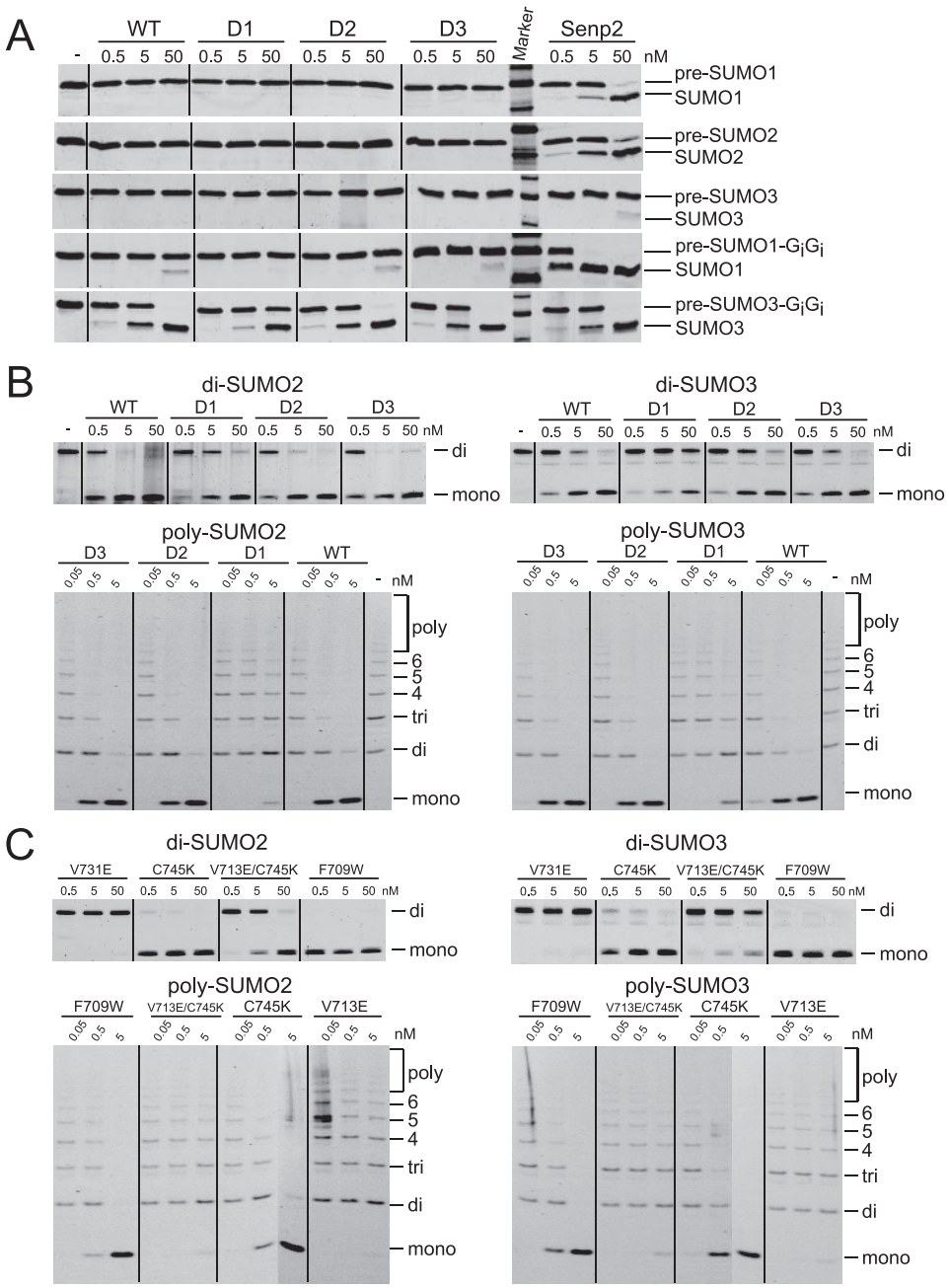

FIGURE 5. **SENP7 mutational analysis and the effects on catalytic function.** *A*, end point assays to detect activities for SENP7 wild-type (*WT*), SENP7-ΔLoop-1 (*D1*), SENP7-ΔLoop-2 (*D2*), SENP7-ΔLoop-3 (*D3*), and SENP2 at 0.5, 5, and 50 nM using the substrates pre-SUMO1, pre-SUMO2, pre-SUMO3, pre-SUMO1-GGG_iG_i-*X*, and pre-SUMO3-GGG_iG_i-*X* at 5 μM. *B*, end point assays to detect deconjugation of di-SUMO2 and di-SUMO3 at 2 μM (*upper panel*), poly-SUMO2, and poly-SUMO3 chains at 45 μg/ml (*lower panel*) using SENP7 wild-type (*WT*), SENP7-ΔLoop-1 (*D1*), SENP7-ΔLoop-2 (*D2*), and SENP7-ΔLoop-3 (*D3*) at 0.05, 0.5, 5, and 50 nM. *C*, end point assays to detect deconjugation of di-SUMO2 and di-SUMO3 at 2 μM (*upper panel*), poly-SUMO2, and poly-SUMO3 chains at 45 μg/ml (*lower panel*) using SENP7 protein containing the following point mutations (V713E, C745K, V713E/C745K, and F709W) at 0.05, 0.5, 5, and 50 nM. For end point assays, reactions were stopped after 10 min with SDS loading buffer and analyzed by PAGE. Proteins were detected by staining with SYPRO or FLAMINGO (Bio-Rad).

pre-SUMO2, and pre-SUMO3. As observed before (Fig. 1), only SENP2 was competent for processing. Addition of two glycine residues after the Gly-Gly motif improved maturation rates slightly for SENP7 with pre-SUMO1-GGG_iG_i-*X*, whereas processing rates improved substantially if pre-SUMO3-GGG_iG_i-*X* was used as the substrate (Fig. 5*A*). Deletion of Loop-1 (*D1* in Fig. 5*A*) reduced processing rates in comparison with wild-type SENP7 or SENP7 containing deletions in either Loop-2 or Loop-3 (Fig. 5*A*).

SENP7 and respective mutant isoforms were next assessed for their ability to deconjugate di-SUMO2/3 and poly-SUMO2/3 substrates using end point assays and different enzyme concentrations (0.05, 0.5, 5, or 50 nM) with 2 μM di-SUMO2/3 or the equivalent mass of poly-SUMO2/3 (Fig. 5*B*). SENP7-ΔLoop-1 was less able to deconjugate di-SUMO2/3 or poly-SUMO2/3 in comparison with either SENP7 or SENP7 that contained deletions of either Loop-2 or Loop-3. These results are consistent with the position of Loop-1 in our structure, which suggests it would project toward the binding surface for SUMO substrates in site A (Fig. 4*D*).

The importance of individual amino acid residues in determining specificity was assessed by substituting Val-713, Cys-745, and Phe-709 to amino acid side chains that are conserved in SENP1 and SENP2. Enzyme titrations and end point assays for di-SUMO2/3 and poly-SUMO2/3 deconjugation were conducted using SENP7, SENP7-V713E, SENP7-C745K, SENP7-F709W, or SENP7-V713E/C745K (Fig. 5*C*). In comparison with wild-type SENP7, deconjugation rates were reduced for SENP7-V713E, whereas SENP7-C745K did not alter deconjugation rates in comparison with wild-type SENP7 (Fig. 5*B*). It is interesting that C745K substitution partially rescued defects observed for SENP7-V713E when present as a double point substitution (SENP7-V713E/C745K). The reduction in deconjugation rates for SENP7-V713E was greater than that observed for SENP7-ΔLoop1 (Fig. 5). Val-713 is located adjacent to Loop-1 where it could interact with SUMO2/3 in site A (Fig. 4*D*), but rather than provide polar interactions with SUMO as observed in complexes with SENP1 and SENP2, our docking analysis suggests that Val-713 might be in a suitable position to provide apolar contacts to the aliphatic portion of the Arg-61 side chain in SUMO2 (Fig. 4*D*).

With the exception of SENP6 and SENP7, all other SENP/ULP family members include a conserved tryptophan side

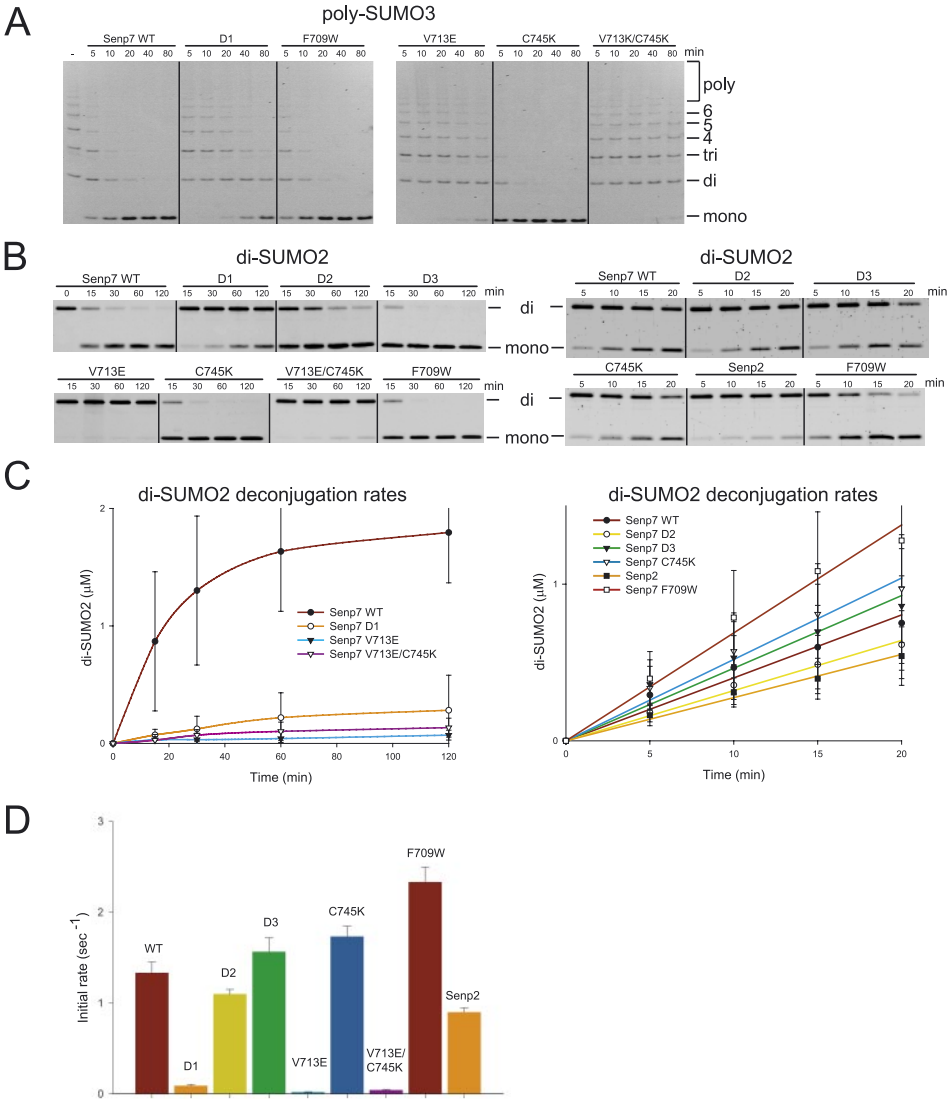

FIGURE 6. **Mutational and kinetic analysis for poly-SUMO3 deconjugation and initial rate measurements during di-SUMO2 deconjugation.** *A,* time course analysis for poly-SUMO3 deconjugation at 45 μg/ml using SENP7 WT, SENP7-ΔLoop-1 (*D1*), SENP7 F709W, SENP7-V713E, SENP7-C745K, and SENP7-V713E/C745K at 0.5 nM. Time intervals indicated in minutes above the respective lane. *B,* time course analysis for di-SUMO2 and di-SUMO2 deconjugation at 2 μM using 0.5 nM SENP7 wild-type or indicated mutants as in *A*. For kinetic analysis, reactions were stopped at the respective time interval with (SDS)-polyacrylamide loading buffer and analyzed by PAGE. Proteins were detected by staining with SYPRO or FLAMINGO (Bio-Rad). Time intervals are indicated in minutes at the *top* of each panel. Mutants exhibiting slower reaction kinetics are depicted on the *left,* and those exhibiting faster kinetics are shown on the *right*. *C,* analysis of the deconjugation rates as determined by quantifying data obtained in *B* for data obtained using longer (*left panel*) or shorter (*right panel*) time intervals. *Axes* are labeled, and *error bars* were obtained by conducting the assays in triplicate. Error bars indicate ±1 S.D. *D, bar* representation for initial rate velocities for rates determined within a linear range from data obtained in *C* for di-SUMO2 deconjugation by SENP7 or indicated SENP7 mutant isoforms.

chain above the active site. In SENP6 and SENP7, this position is conserved as phenylalanine (Fig. 3*D*). Because previous studies suggested that the tryptophan residue played an important role in positioning both peptide and isopeptide substrates over the SENP/ULP active site (34), we substituted SENP7 Phe-709 to tryptophan and analyzed the effect of this substitution on deconjugation and processing. End point deconjugation reactions using di-SUMO2/3 or poly-SUMO2/3 revealed rates equivalent to or slightly greater than wild-type SENP7 (Fig. 5*C*), although SENP7-F709W substitution resulted in a 2-fold higher activity when di-SUMO2 deconjugation rates were measured (see below; Fig. 6). Although these effects were minimal, SENP7-F709W substitution enhanced SUMO processing activities when compared with wild-type SENP7 (supplemental Fig. 3).

The effects of individual mutations were next assessed by time course analysis for poly-SUMO2/3 deconjugation using SENP7 and the respective mutant isoforms to determine the relative rates for deconjugation at fixed concentrations of enzyme and substrate (Fig. 6*A*; see "Experimental Procedures"). These data corroborated observations made during end point assays but resulted in more evident rate reductions for SENP7-ΔLoop-1 and SENP7-V713E. To obtain a more quantitative assessment for these differences, di-SUMO2 was utilized at 2 μM in reactions containing 0.5 nM SENP7 or respective SENP7 mutant isoforms (Fig. 6*B*). For mutants exhibiting slower kinetics, longer time intervals were utilized (Fig. 6*B*, *left panel*) in comparison with those used for wild-type and other SENP7 mutant isoforms (Fig. 6*B*, *right panel*). Compared with wild-type SENP7, SENP7ΔLoop-1 or SENP7-V713E elicited 15- or 65-fold reductions in deconjugation rates, respectively. In this case, introduction of the C745K substitution within SENP7-V713E/C745K did not rescue defects observed for SENP7-V713E. Differences in activity were observed for other SENP7 mutant isoforms, and although most were deemed insignificant, it is worth noting that SENP7-F709W exhibited 2-fold faster rates in these assays under the conditions tested. Perhaps most interesting was the observation that SENP7 catalyzed di-SUMO2 deconjugation at rates faster than SENP2. This is in stark contrast to results obtained for deconjugation reactions containing SUMO1 or processing reactions with pre-SUMO1, pre-SUMO2, or pre-SUMO3 (Fig. 1).

DISCUSSION

Of the six human SENP/ULP proteases dedicated to cleavage and processing of SUMO, SENP6 and SENP7 are the most divergent with respect to primary sequence and structure. We have demonstrated that SENP6 and SENP7 catalytic domains display a preference for SUMO deconjugation over processing, and deconjugation of substrates containing SUMO2/3 was pre-

TABLE 2

Summary for catalytic activities observed for SENP2, SENP6, and SENP7 and mutational effects on SENP7 activity

Relative activities approximated by symbols for each SENP isoform are as follows: – (none); +/− (weak); + (some); ++ (good); +++ (very good); and ++++ (excellent). SENP isoforms are denoted by 2 (SENP2), 6 (SENP6), and 7 (SENP7) with SENP7 mutant isoforms denoted by 7-D1 (SENP7(Δ685–692)), 7-D2 (SENP7(Δ748–767)), and L-D3 (SENP7(Δ811–861)). SENP7 containing single or double point mutations is indicated by 7- followed by V731E, C745K, V731E/C745K, and F709W.

SENP isoform	2	6	7	7-D1	7-D2	7-D3	7-F709W	7-V731E	7-C745K	7-V731E/C745K
Di-SUMO2	++	++++	++	+	++	++	++++	−	++	+/−
Di-SUMO3	++	++++	++	+	++	++	++++	−	++	+/−
Poly-SUMO2	++	++++	+++	+	+++	+++	+++	−	+++	+/−
Poly-SUMO3	++	++++	+++	+	+++	+++	+++	−	+++	+/−
Pre-SUMO1	+	−	−	−	−	−	−			
Pre-SUMO2	++	+/−	−	−	−	−	+/−			
Pre-SUMO3	+	−	−	−	−	−	−			
Pre-SUMO1G_iG_i	+++	−	+/−	−	+/−	+/−	+			
Pre-SUMO2G_iG_i	+++	++	++							
Pre-SUMO3G_iG_i	++	+	+	+/−	+	+	++			
RG-SUMO1	++++	+	+/−							
RG-SUMO2/3	++++	++	++							

ferred over substrates containing SUMO1. Furthermore, SENP6 and SENP7 exhibit higher rates for deconjugating di-SUMO2/3 or poly-SUMO2/3 in comparison with deconjugation of SUMO2/3-conjugated RanGAP1. It is also worth noting that SENP6 was much more proficient in these activities when compared with those catalyzed by SENP7 (summarized in Table 2).

Our structural analysis revealed that SENP7 is a *bona fide* member of the SENP/ULP protease family, although structural comparisons to other well characterized family members such as SENP1, SENP2, and ULP1 revealed significant differences at the structural and primary sequence level. These include four sequence insertions (Loop-1 through Loop-4) conserved in SENP6 and SENP7 that have correlates in the SENP7 structure. Loop-1 and Loop-2 are situated on the protease surface in positions predicted to interact with SUMO in binding site A (Fig. 4), and whereas deletion of Loop-2 had no effect on SENP7 activities in the present analysis, deletion of Loop-1 resulted in lower activities for all of the substrates tested. Primary sequence alignment suggests that Loop-1 is conserved in SENP6 and SENP7 but absent in all other SENP/ULP family members. Immediately adjacent to Loop-1 is Val-713, a residue conserved in SENP6 and SENP7. When this residue was substituted to glutamate (conserved in SENP1 and SENP2), SENP7 activity was diminished in comparison with wild-type SENP7. It is worth noting that polar residues at this analogous position in structures of SENP1, SENP2, and ULP1 participate in direct contacts to arginine side chains conserved in human SUMO1, SUMO2/3, and yeast SMT3 (33–35, 44, 45).

A recent study noted that SENP6 and SENP7 exhibited unexpected preferences for short SUMO-derived synthetic substrates that contained arginine at position P3 (three amino acid residues prior to the C-terminal glycine) (46). What is striking about this observation is that this position is almost always conserved as threonine in SUMO, whereas arginine is observed in this position in ubiquitin. These data led the authors to muse that SENP6 and SENP7 may not be SUMO-specific enzymes (46). Our biochemical results suggest that SENP6 and SENP7 catalytic domains are excellent SUMO enzymes for deconjugating di-SUMO2/3 and poly-SUMO2/3, and our structural analysis identified unique elements within this SENP/ULP subfamily that contribute to function during SUMO deconjugation and processing.

SENP6 and SENP7 exhibited higher activities during deconjugation of poly-SUMO2/3 chains, even when compared with activities catalyzed by the SENP2 catalytic domain. Whereas Loop-3 appears to be in a suitable position to explain this specificity via interactions with an extended SUMO chain (Fig. 4*B*), deletion of Loop-3 had no effect on the activities of SENP7 under the conditions tested. With that said, it is important to note that SENP6 and SENP7 were also able to deconjugate SUMO2/3-RanGAP1 at rates comparable with SENP2, suggesting that high poly-SUMO2/3 chain deconjugation activities observed for SENP6 and SENP7 may simply reflect a preference for flexible isopeptide linked substrates in site A and site B. Although additional work will be required to determine the physical basis for chain specificity as it pertains to SENP6 and SENP7 activities in the cell, the present analysis has revealed unique determinants within the SENP6/7 subfamily that contribute to substrate specificity and catalytic activity.

Acknowledgments—Use of the Advanced Photon Source was supported by the United States Department of Energy, Office of Science, Office of Basic Energy Sciences, under Contract W-31-109-Eng-38. Use of the NE-CAT beamline at Sector 24 is based upon research conducted at the Northeastern Collaborative Access Team beamlines of the Advanced Photon Source, which is supported by National Institute of Health Grant RR-15301 from the NCRR.

REFERENCES

1. Hershko, A., and Ciechanover, A. (1998) *Annu. Rev. Biochem.* **67,** 425–479
2. Kerscher, O., Felberbaum, R., and Hochstrasser, M. (2006) *Annu. Rev. Cell Dev. Biol.* **22,** 159–180
3. Geiss-Friedlander, R., and Melchior, F. (2007) *Nat. Rev. Mol. Cell Biol.* **8,** 947–956
4. Johnson E. S. (2004) *Annu. Rev. Biochem.* **73,** 355–382
5. Bohren, K. M., Nadkarni, V., Song, J. H., Gabbay, K. H., and Owerbach, D. A. (2004) *J. Biol. Chem.* **279,** 27233–27238
6. Owerbach, D., McKay, E. M., Yeh, E. T., Gabbay, K. H., and Bohren, K. M. (2005) *Biochem. Biophys. Res. Commun.* **337,** 517–520
7. Li, S.-J., and Hochstrasser, M. (1999) *Nature* **398,** 246–251
8. Saitoh, H., and Hinchey, J. (2000) *J. Biol. Chem.* **275,** 6252–6258
9. Vertegaal, A. C., Andersen, J. S., Ogg, S. C., Hay, R. T., Mann, M., and Lamond, A. I. (2006) *Mol. Cell. Proteomics* **5,** 2298–2310
10. Ayaydin, F., and Dasso, M. (2004) *Mol. Biol. Cell* **15,** 5208–5218
11. Bossis, G., and Melchior, F. (2006) *Mol. Cell* **21,** 349–357
12. Tatham, M. H., Jaffray, E., Vaughan, O. A., Desterro, J. M., Botting, C. H.,

Naismith, J. H., and Hay, R. T. (2001) *J. Biol. Chem.* **276,** 35368–35374
13. Cheng, C. H., Lo, Y. H., Liang, S. S., Ti, S. C., Lin, F. M., Yeh, C. H., Huang, H. Y., Wang, T. F., and Cheng, C. H. (2006) *Genes Dev.* **20,** 2067–2081
14. Bylebyl, G. R., Belichenko, I., and Johnson, E. S. (2003) *J. Biol. Chem.* **278,** 44113–44120
15. Li, Y., Wang, H., Wang, S., Quon, D., Liu, Y. W., and Cordell, B. (2003) *Proc. Natl. Acad. Sci. U. S. A.* **100,** 259–264
16. Fu, C., Ahmed, K., Ding, H., Ding, X., Lan, J., Yang, Z., Miao, Y., Zhu, Y., Shi, Y., Zhu, J., Huang, H., and Yao, X. (2005) *Oncogene* **24,** 5401–5413
17. Tatham, M. H., Geoffroy, M. C., Shen, L., Plechanovova, A., Hattersley, N., Jaffray, E. G., Palvimo, J. J., and Hay, R. T. (2008) *Nat. Cell Biol.* **10,** 538–546
18. Lallemand-Breitenbach, V., Jeanne, M., Benhenda, S., Nasr, R., Lei, M., Peres, L., Zhou, J., Zhu, J., Raught, B., and de Thé, H. (2008) *Nat. Cell Biol.* **10,** 547–555
19. Mukhopadhyay, D., and Dasso, M. (2007) *Trends Biochem. Sci.* **32,** 286–295
20. Gan-Erdene, T., Nagamalleswari, K., Yin, L., Wu, K., Pan, Z. Q., and Wilkinson, K. D. (2003) *J. Biol. Chem.* **278,** 28892–28900
21. Wu, K., Yamoah, K., Dolios, G., Gan-Erdene, T., Tan, P., Chen, A., Lee, C. G., Wei, N., Wilkinson, K. D., Wang, R., and Pan, Z. Q. (2003) *J. Biol. Chem.* **278,** 28882–28891
22. Reverter, D., Wu, K., Erdene, T. G., Pan, Z. Q., Wilkinson, K. D., and Lima, C. D. (2005) *J. Mol. Biol.* **345,** 141–151
23. Shen, L. N., Liu, H., Dong, C., Xirodimas, D., Naismith, J. H., and Hay, R. T. (2005) *EMBO J.* **24,** 1341–1351
24. Yamaguchi, T., Sharma, P., Athanasiou, M., Kumar, A., Yamada, S., and Kuehn, M. R. (2005) *Mol. Cell Biol.* **25,** 5171–5182
25. Cheng, J., Kang, X., Zhang, S., and Yeh, E. T. (2007) *Cell* **131,** 584–595
26. Di Bacco, A., Ouyang, J., Lee, H. Y., Catic, A., Ploegh, H., and Gill, G. (2006) *Mol. Cell Biol.* **26,** 4489–4498
27. Bailey, D., and O'Hare, P. (2004) *J. Biol. Chem.* **279,** 692–703
28. Hang, J., and Dasso, M. (2002) *J. Biol. Chem.* **277,** 19961–19966
29. Nishida, T., Tanaka, H., and Yasuda, H. (2000) *Eur. J. Biochem.* **267,** 6423–6427
30. Zhang, H., Saitoh, H., and Matunis, M. J. (2002) *Mol. Cell Biol.* **22,** 6498–6508
31. Gong, L., and Yeh, E. T. T. (2006) *J. Biol. Chem.* **281,** 15869–15877
32. Mukhopadhyay, D., Ayaydin, F., Kolli, N., Tan, S. H., Anan, T., Kametaka, A., Azuma, Y., Wilkinson, K. D., and Dasso, M. (2006) *J. Cell Biol.* **174,** 939–949
33. Reverter, D., and Lima, C. D. (2004) *Structure* (*Lond.*) **12,** 1519–1531
34. Reverter, D., and Lima, C. D. (2006) *Nat. Struct. Mol. Biol.* **13,** 1060–1068
35. Shen, L., Tatham, M. H., Dong, C., Zagorska, A., Naismith, J. H., and Hay, R. T. (2006) *Nat. Struct. Mol. Biol.* **13,** 1069–1077
36. Mikolajczyk, J., Drag, M., Békés, M., Cao, J. T., Ronai, Z., and Salvesen, G. S. (2007) *J. Biol. Chem.* **282,** 26217–26224
37. Otwinowski, Z., and Minor, W. (1997) *Methods Enzymol.* **276,** 307–326
38. CCP4 (1994) *Acta Crystallogr. Sect. D* **50,** 760–763
39. Terwilliger, T. C., and Berendzen, J. (1999) *Acta Crystallogr. Sect. D* **55,** 849–861
40. Jones, T. A., Zou, J. Y., Cowan, S. W., and Kjeldgaard, M. (1991) *Acta Crystallogr. Sect. A* **47,** 110–118
41. Emsley, P., and Cowtan, K. (2004) *Acta Crystallogr. Sect. D* **60,** 2126–2132
42. Brünger, A. T., Adams, P. D., Clore, G. M., Delano, W. L., Gross, P., Grossekunstleve, R. W., Jiang, J. S., Kuszewski, J., Nilges, M., Pannu, N. S., Read, R. J., Rice, L. M., Simonson, T., and Warren, G. L. (1998) *Acta Crystallogr. Sect. D* **54,** 905–921
43. Davis, I. W., Leaver-Fay, A., Chen, V. B., Block, J. N., Kapral, G. J., Wang, X., Murray, L. W., Arendall, W. B., III, Snoeyink, J., Richardson, J. S., and Richardson, D. C. (2007) *Nucleic Acids Res.* **35,** W375–W383
44. Mossessova, E., and Lima, C. D. (2000) *Mol. Cell* **5,** 865–876
45. Xu, Z., Chau, S. F., Lam, K. H., Chan, H. Y., Ng, T. B., and Au, S. W. (2006) *Biochem. J.* **398,** 345–352
46. Drag, M., Mikolajczyk, J., Krishnakumar, I. M., Huang, Z., and Salvesen, G. S. (2008) *Biochem. J.* **409,** 461–469
47. DeLano, W. L. (2002) PyMOL, Version 0_99rc6, DeLano Scientific, San Carlos, CA
48. Weiss, M. S. (2001) *J. Appl. Crystallogr.* **34,** 130–135